Surface Viscosity, Diffusion, and Intermonolayer Friction: Simulating Sheared Amphiphilic Bilayers

S. A. Shkulipa, W. K. den Otter, and W. J. Briels
Computational Dispersion Rheology, Faculty of Science and Technology, University of Twente, 7500 AE Enschede, The Netherlands

ABSTRACT The flow properties of an amphiphilic bilayer are studied in molecular dynamics simulations, by exposing a coarse grained model bilayer to two shear flows directed along the bilayer surface. The first field, with a vorticity perpendicular to the bilayer, induces a regular shear deformation, allowing a direct calculation of the surface viscosity. In experiments this property is measured indirectly, by relating it to the diffusion coefficient of a tracer particle through the Saffman-Einstein expression. The current calculations provide an independent test of this relation. The second flow field, with a vorticity parallel to the bilayer, causes the two constituent monolayers to slide past one another, yielding the interlayer friction coefficient.

INTRODUCTION

Amphiphilic bilayers and biological membranes are planar self-assembled aggregates of amphiphilic molecules, such as surfactants or lipids, in which a hydrophilic headgroup is covalently bound to a hydrophobic tail. These structures are locally flat, but smoothly undulating on a length scale well beyond their thickness (1,2). Because bilayers are held together by relatively weak nonbonded interaction forces, they behave in many respects as two-dimensional liquids suspended in a three-dimensional solvent matrix. This makes bilayers very susceptible to external forces, which give rise to deformations of the overall shape of the bilayer and to flow within the bilayer. Examples hereof include the elongation and rupture of vesicles sucked into a pipette (3,4), the shear induced transition of a stack of bilayers into an onion-like structure (5–8), the large changes in shape of red blood cells as they creep through narrow passageways (9), the resilience of a cell when prodded by a needle, and the pulling of tethers from a vesicle by a localized force (10–15). In this article we will concentrate on deformations that preserve the overall shape of the bilayer.

A flat or weakly undulating bilayer oriented parallel to the xy plane (see Fig. 1) can be exposed to two distinct flow deformations, as illustrated in Fig. 2. The first flow field, $\mathbf{v}(\mathbf{x}) = (\dot{\boldsymbol{\gamma}}\, y, 0, 0)$, describes the linear velocity profile of a regular shear flow with a shear rate $\dot{\boldsymbol{\gamma}}$. Following the convention in the literature on sheared block copolymers (16), this flow is referred to as a perpendicular shear flow. The resistance of the bilayer against this flow is characterized by a two-dimensional surface viscosity, η_s, which, analogous to the regular three-dimensional viscosity, relates the shear force per unit of length of bilayer to the shear rate. Note that both leaflets of the bilayer move in unison under this field. In the so-called parallel flow field, $\mathbf{v}(\mathbf{x}) = (\dot{\boldsymbol{\gamma}}\, z, 0, 0)$, on the other hand, the two monolayers of the bilayer are sliding past one another as two flat rigid objects with velocities $\pm\Delta v\hat{\mathbf{e}}_x$. A friction coefficient, ξ, is defined by the ratio between the sliding force per unit of bilayer area and the velocity difference between the two leaflets.

The viscosity and friction coefficient are not easily accessible under experimental conditions. Forced deformations of a bilayer frequently culminate in the simultaneous occurrence of both flow fields, and are often accompanied by bending and stretching of the bilayer. Nonuniform stress distributions resulting in diffusion-like stress relaxation processes, both within and between (''flip-flops'') the monolayers, further complicate the interpretation of the experimental data. For an extensive discussion of these processes, we refer the reader to Evans and co-workers (10,15).

Viscosity measurements by pulling a tether from a vesicle, for instance, are hampered by the above effects. It proves more convenient, therefore, to deduce the viscosity from the translational and rotational diffusion coefficients of fluorescent transmembrane tracer particles in a quiescent bilayer (see Waugh (14) and references cited therein) using a Stokes-Einstein type expression derived for this particular system by Saffman (17). Saffman elegantly solved Stokes' equations of the creeping flow around a cylinder (i.e., the tracer) moving in a thin sheet of viscous liquid (i.e., the bilayer), by emphasizing the role played by the liquid, of viscosity η_w, on either side of this sheet. Falling ball viscosimetry (18), in which a microsphere moving under gravity is constrained to a bilayer vesicle, is essentially based on the same theory. An independent validation of the Saffman-Einstein expression for use with bilayers is therefore welcomed.

Friction coefficients have been measured by pulling a thin tether from a vesicle (10–12,15), where the sharp change in curvature at the vesicle-tether junction induces a velocity difference between the inner and outer layers. A second method focuses on the slip occurring when amphiphiles flow through an hourglass-shaped fusion pore from a bilayer under low surface tension to a bilayer under a higher tension

Submitted March 11, 2005, and accepted for publication May 2, 2005.

Address reprint requests to W. K. den Otter, Faculty of Science and Technology, University of Twente, PO Box 217, 7500 AE Enschede, The Netherlands. E-mail: w.k.denotter@utwente.nl.

0006-3495/05/08/823/07 $2.00

doi: 10.1529/biophysj.105.062653

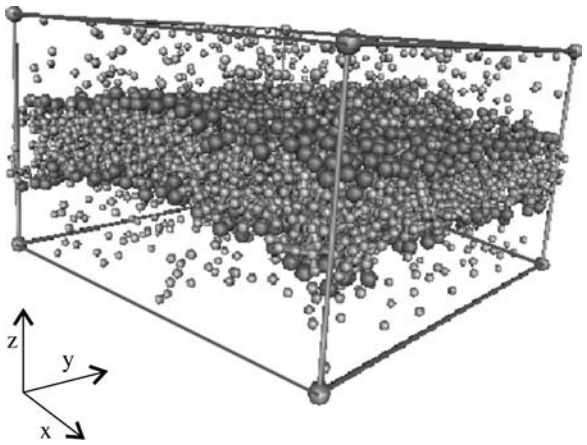

FIGURE 1 A snapshot of the bilayer-liquid simulation box. The number of surrounding solvent particles has been reduced for clarity.

(19). The wide range of the few reported friction coefficients illustrates the complexity of (the interpretation of) these ingenious measurements, and the sensitivity to the amphiphiles used in the experiment.

The objective of this article is to establish methods to determine both the shear viscosity and the friction coefficient of a bilayer by means of computer simulations on the molecular level. Bilayers have been the subject of numerous modeling studies, which for the most part focused on the equilibrium properties and on the self-assembly from a disordered amphiphilic solution (20–25). To the best of our knowledge, the flow behavior of a bilayer has never been simulated at this level. Because our aim here is to develop and validate new techniques, we opted for a relatively simple and fast coarse-grained amphiphilic model known to reproduce realistic thermodynamic properties (26–30). No claims are made to the applicability of the model to calculate realistic values of dynamical properties. Our aim is to develop methods and to test the applicability of the Saffman-Einstein equation. The model and other simulation details are summarized in the ''Setup'' section. Results are presented in the ''Results'' section, where we describe the response of the bilayer, and of the individual amphiphiles, to the applied flow fields. We end with a discussion of the applied methods, and a comparison with the available experimental data, in the ''Discussion and Conclusions'' section.

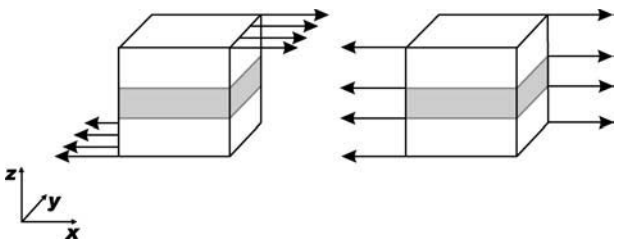

FIGURE 2 Side views of the simulated system, highlighting parallel (*left*) and perpendicular (*right*) shear flows.

SETUP

The speed of coarse-grained (CG) simulation models makes these models very attractive for simulations requiring large length and timescales, where fully atomistic models are computationally too demanding, and to put new simulation techniques to the test, as is the case here. In coarse-grained models, a number of atoms is grouped together to form a CG particle. The equation of motion of the CG particle follows, in principle, by averaging over the dynamics of the constituent atoms (31). The resulting Langevin equation combines conservative forces with friction and random forces (32). The conservative forces are responsible for the thermodynamic properties of the CG model, and therefore deservedly lie at the heart of the currently available fitting procedures (22,24,28). In case one restricts attention to structural and thermodynamic properties, the precise values of the friction and random forces are irrelevant. Of course, as soon as one wants to calculate realistic dynamical properties, the precise nature of these forces matters a lot. Unfortunately it is still not fully understood how to calculate friction and random forces from atomistic simulations (31,33). As was already mentioned in the Introduction, however, our aim is primarily to develop and test methods to study the flow properties of a bilayer. We therefore decided to use a simplified CG model, in which friction and random forces are neglected altogether.

The simulation model we used was developed by Goetz and Lipowsky (27,28). They chose an amphiphilic architecture in which the head is represented by a single bead (h) and the tail is reduced to four beads (t) representing roughly three CH_2 units each. The solvent consists of loose water beads (w), corresponding with two water molecules. Interactions between like particles, as well as the hydrophilic head-water interactions, are modeled by a Lennard-Jones potential, $\Phi_{LJ}(r) = 4\epsilon[(r/\sigma)^{-12} - (r/\sigma)^{-6}]$, with $\epsilon = 2$ kJ/mol and $\sigma = 1/3$ nm. The hydrophobic tail-water and tail-head interactions are modeled by a purely repulsive potential, $\Phi_{rep}(r) = \epsilon[r/(1.05\sigma)]^{-9}$. The nonbonded forces are implemented in a shifted-force fashion, ensuring a smooth truncation of the energy and the force at the cut-off distance of 2.5 σ. The particles of the amphiphilic molecules are held together by harmonic bond potentials, $\Phi_{bond}(l) = 5000\epsilon\sigma^{-2}(l - \sigma)^2$. An angle potential between every set of three consecutively bonded particles, $\Phi_{angle}(\phi) = 2\epsilon[1 - \cos(\phi)]$, introduces a bending stiffness. There are no dihedral potentials. All particles have the same mass m of 36 a.u., and the number density is 2 particles per 3 σ^3. In all our simulations the temperature T was 325 K, or 1.35 ϵ/k_B with k_B Boltzmann's constant, and was maintained by means of a Nosé-Hoover thermostat. The time step used in the Verlet leapfrog scheme was $\tau/500$, where $\tau = \sqrt{m\sigma^2/\varepsilon}$ is the unit of time. Previous simulations with this CG model showed that its equilibrium area, elastic modulus, bending rigidity, and line tension coefficient compare favorably with experimental data (26–30). All simulations were run using the

DL_POLY_2.0 package (34), tailored to the specifications of the problem.

Rectangular periodic simulation boxes were used, each having a square ground plane of sides $L_\parallel$ parallel to the bilayer and the xy plane, and a height $L_\perp$ perpendicular to these. Initial bilayer-solvent configurations were created by constructing two parallel square lattice layers of straight amphiphilic molecules, 1152 in total, with their heads pointing outward. The 10,800 solvent particles were placed at random in the box, taking care to avoid overlap with the bilayer and with previously inserted solvent particles. The boxes were then energy minimized for a limited number of steps, followed by equilibration runs at the desired temperature. A snapshot of the resulting bilayer box is shown in Fig. 1. On varying $L_\parallel$ it was found that at $L_\parallel = 34.9\ \sigma$ the bilayer is in the tensionless state, in which the average pressures parallel and perpendicular to the bilayer are identical, to wit, $\sim 1.5\epsilon\sigma^{-3}$ or 1.4 kbar. The structure factors S of the thermal undulations followed the theoretical prediction for the tensionless state, $S(\mathbf{q}) \propto \mathbf{q}^{-4}$, with $\mathbf{q}$ a wave vector commensurate with the box dimension $L_\parallel$ (1,2,27). The box height of 20.4 σ allows the solvent enough freedom to reach an isotropic pressure in the middle between two periodic images of the bilayer (28).

Simulations under shear rate $\dot\gamma$ were run using Lees-Edwards boundary conditions (35,36), such that the flow was directed along the x axis, i.e., such that $\mathbf{v}(\mathbf{x}) = v(\mathbf{x})\hat{\mathbf{e}}_x$. For homogeneous solvent boxes the shear direction is of course irrelevant, but this is no longer the case for boxes with a bilayer. A perpendicular flow was generated such that $v_\perp(\mathbf{x}+L_\parallel\hat{\mathbf{e}}_y) = v_\perp(\mathbf{x})+\dot\gamma L_\parallel$ and a parallel flow such that $v_\parallel(\mathbf{x}+L_\perp\hat{\mathbf{e}}_z) = v_\parallel(\mathbf{x})+\dot\gamma L_\perp$. Analogous flow fields along the y axis produce identical results. The Nosé-Hoover thermostat (35) was adapted for these shear conditions, by calculating the temperature from the velocity distribution relative to the local flow field and by rescaling only superficial velocities. In these calculations the flow fields were assumed to be given by appropriate linear expressions, although some runs yielded a distinctly nonlinear profile. Using the actual flow field in the thermostating routine did not significantly change the results. The structure factors $S(\mathbf{q})$ of the thermal undulations of the bilayer still scaled as $\mathbf{q}^{-4}$ under shear, suggesting that the flow does not induce any significant tension on the bilayer. After turning on the shear flow, the simulations were continued until all transient effects had died out and a steady laminar flow field had formed, before starting the production runs.

Three techniques were used to determine the overall shear viscosities of the simulated systems (35). In the nonsheared runs, the viscosity η_{tot} was calculated using the Green-Kubo relation

$$\eta_{\text{tot}} = \frac{V}{k_B T}\int_0^\infty \langle P_{\alpha\beta}(t)P_{\alpha\beta}(0)\rangle\, dt, \tag{1}$$

where $P_{\alpha\beta}$ is an off-diagonal ($\alpha \neq \beta$) element of the pressure tensor, V is the volume of the box, and the angular brackets denote a canonical average. For a sheared system the viscosity is defined as the ratio between the total shear force per unit area and the shear rate,

$$\eta_{\text{tot}} \equiv \frac{F_{\text{shear}}/A}{\dot\gamma} = \frac{\langle P_{\alpha\beta}\rangle}{\dot\gamma}. \tag{2}$$

For systems containing a bilayer we use $\alpha = x$ and $\beta = y$ or z for the perpendicular and parallel shear flows, respectively. The third method is based on the realization that the rate of energy production, $\eta_{\text{tot}}\dot\gamma^2 V$, by the shearing boundaries is easily calculated as the time derivative, $\dot E$, of the extended Hamiltonian of the system plus thermostat, to arrive at

$$\eta_{\text{tot}} = \frac{\dot E}{\dot\gamma^2 V}. \tag{3}$$

Notice that in the stationary state the energy of the system is constant and therefore $\dot E$ is equal to the rate of energy extraction from the system by the thermostat. A similar approach was recently proposed by Holian (37). The conversion from total shear viscosities into the viscosity and friction coefficient of the bilayer will be discussed at the appropriate places in the next section.

RESULTS

We start with the viscosity of the solvent. Two boxes were filled randomly with 2250 and 66,667 solvent particles, respectively. For both boxes and for all three calculation methods mentioned in the previous section, we found a viscosity η_w of just over $1.0\epsilon^{1/2}m^{1/2}\sigma^{-2}$, virtually independent of the applied shear rate $\dot\gamma$ ranging from zero to $0.2\ \tau^{-1}$. This value translates into 1.3×10^{-4} Pa s, which amounts to about one-quarter of the experimental viscosity of 5×10^{-4} Pa s for water at this temperature. The diffusion coefficient of the solvent particles was found to be $0.1\sigma^2/\tau$, or 1×10^{-8} m^2/s, which is about four times larger than the experimental self-diffusion coefficient, 2.5×10^{-9} m^2/s, of a water molecule at this temperature.

Using the same approaches, the viscosity of a homogeneous liquid of chains of five particles, t_5, was found to be $\eta_b \approx 2.1\epsilon^{1/2}m^{1/2}\sigma^{-2}$, twice the value obtained for the solvent, again independent of the shear rate. For comparison, the experimental viscosity of a comparable liquid of hydrocarbon chains, n-hexadecane, is about eight times higher (38). These results indicate that the model is not well suited to aim for dynamical properties in quantitative agreement with experiments. Marrink et al. (24), following Groot and Rabone (21), addressed the spurious speedup of their coarse-grained model by introducing an ad hoc scaling factor of four to relate the elapsed simulation time to the real time. An alternative physically sound route to solve the dynamical discrepancy is to maintain the friction and random forces in the equations of motion of the coarse-grained particles. In

case these forces grow large relative to the inertial forces, one is of course better off running Brownian dynamics.

Perpendicular shear

Of the two interesting shear directions of a box containing a bilayer, the perpendicularly sheared system will be discussed first. The total viscosity of the system has been calculated for the quiescent box, as well as for those with shear rates ranging from 0.001 to 0.1 τ^{-1}, to be $\sim 1.6\ \epsilon^{1/2} m^{1/2} \sigma^{-2}$ in each case. In the steady state, the velocity distribution of the amphiphilic particles closely follows a linear flow field. This suggests that the bilayer behaves like a regular sheared liquid (be it one in which the molecules are bound to a plane), which is a prerequisite for a well-defined bilayer surface viscosity. Analogous to Eq. 2, the surface viscosity is defined as the total shear force on the bilayer per unit of length, divided by the shear rate,

$$\eta_s \equiv \frac{F_{\text{bilayer}}/L_\parallel}{\dot{\gamma}}, \tag{4}$$

$$F_{\text{bilayer}} = \langle P_{xy} \rangle L_\parallel L_\perp - \eta_w \dot{\gamma} L_\parallel (L_\perp - h_s). \tag{5}$$

The last equation defines the shear force on the bilayer, F_{bilayer}, as the total shear force across the xz plane minus the contribution acting on the solvent, where $h_s \approx 6.8\ \sigma$ is the thickness of the bilayer. The shear viscosity of the bilayer was found to be $\sim 20\ \epsilon^{1/2} m^{1/2} \sigma^{-1}$, or 8.5×10^{-13} Pa m s. Fig. 3 reveals a weak dependence of this value on the shear rate, with a reduction by $\sim 10\%$ over the entire range covered.

Parallel shear

Under a parallel shear field the total viscosity of the box was $\sim 1.4\ \epsilon^{1/2} m^{1/2} \sigma^{-2}$, for shear rates ranging from 0.002 to 0.05 τ^{-1}. A similar value was obtained by applying the Green-Kubo relation to the quiescent box. As in the previous section, we now have to convert this number into a property of the bilayer.

Because of the orientation of the bilayer relative to the sheared boundaries, we expect a velocity profile like the one drawn in Fig. 4. The profile in the solvent will be linear, with a slope $\dot{\gamma}_w$ different from the imposed shear rate $\dot{\gamma}$. In the middle of the box the two leaflets of the monolayer are sliding past one another, like two flat solid objects, with velocities $\pm \Delta v \hat{\mathbf{e}}_x$, giving rise to a friction force between the two leaflets. The friction coefficient of this motion follows from the shearing force F exerted on the top (bottom) monolayer, by the solvent above (below) the bilayer, according to

$$\xi \equiv \frac{2F/L_\parallel^2}{2\Delta v}. \tag{6}$$

All that remains is to determine the two unknowns featuring on the right-hand side of the above expression.

The actually calculated velocity profile (see Fig. 5) shows that the velocity gradient within the bilayer region is considerably smaller than in the solvent, but not zero. This is caused by a convolution of the idealized profile with the thermal undulations of the bilayer. Unfortunately, this renders direct estimates of Δv from the velocity profiles highly inaccurate. The shear rate of the solvent at some distance from the bilayer, however, is not affected by these undulations. Under the assumption of stick boundary conditions at the bilayer-solvent interface, we can calculate the slip velocity from

$$2\Delta v = \dot{\gamma} L_\perp - \dot{\gamma}_w (L_\perp - h_s). \tag{7}$$

This velocity turns out to be proportional to the overall shear rate.

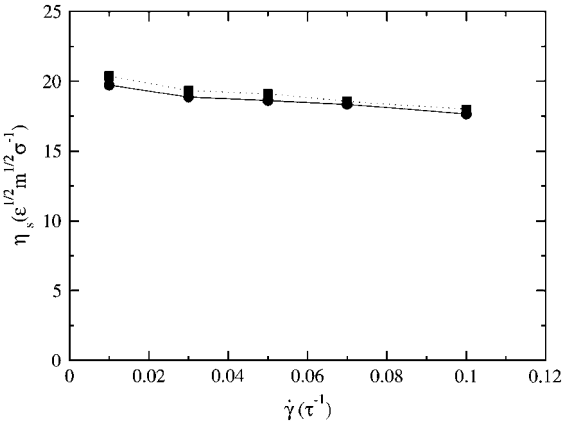

FIGURE 3 The surface viscosity of the bilayer, derived from simulations with a perpendicular shear flow, plotted against the applied shear rate. The data points were obtained by calculating the total shear force on the system, i.e., the first term on the right hand of Eq. 5, from the pressure (●) or from the thermostat (■).

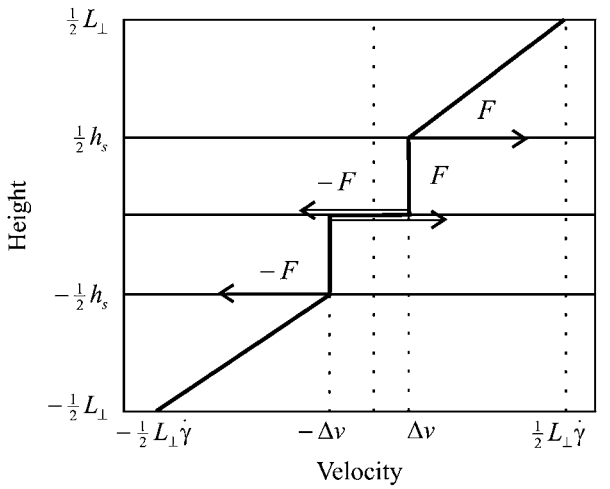

FIGURE 4 Sketch of the velocity profile (*line*) and of the forces (*arrows*) for a bilayer system under parallel shear.

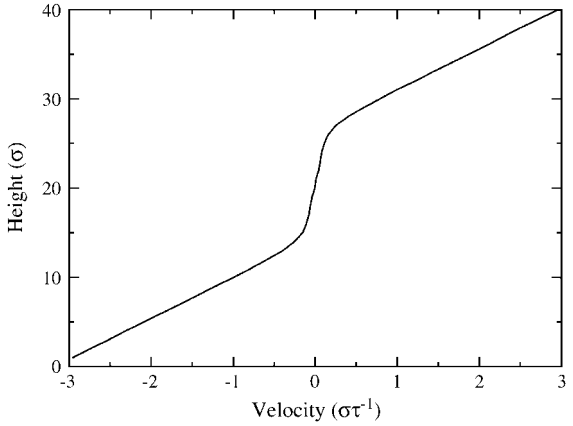

FIGURE 5 Velocity profile of a bilayer system at a parallel shear rate of 0.03 τ^{-1}.

Alternatively, one could look at the distances traveled by the amphiphilic particles, along the flow direction, over the course of a simulation. This distribution is shown in Fig. 6 for the head particles of the two monolayers, excluding a few that flipped from one monolayer to the other. Because of the covalent bonding, the distributions for the tail particles are virtually identical. From the location of the peak, divided by the length of the simulation, we again obtain Δv. The numerical values obtained by both methods agree very well, implying stick boundary conditions at the two bilayer-solvent interfaces. Consequently, the force exerted on the top monolayer by the solvent above the bilayer can be calculated from the shear rate in the solvent, $F = \dot{\gamma}_w \eta_w L_\parallel^2$. Inserting these results in Eq. 6, we find a friction coefficient $\xi = 3.7\ \epsilon^{1/2} m^{1/2} \sigma^{-3}$, or 1.4×10^6 N s m^{-3}. As shown in Fig. 7, this value is effectively independent of the slip velocity.

We end this section with a discussion of structural properties of a bilayer under a parallel shear deformation. Fig. 8

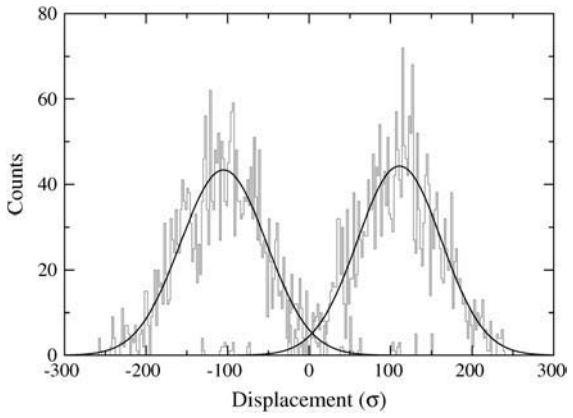

FIGURE 6 Probability distributions of displacements, along the flow direction, of head particles in the top (*right peak*) and bottom (*left peak*) monolayers. At a shear rate of 0.03 τ^{-1}, the amphiphiles cover a distance of nearly three box lengths over a period of ~18,000 τ. The solid lines are Gaussian fits.

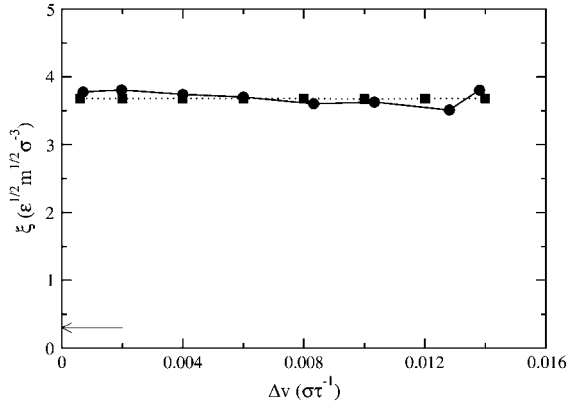

FIGURE 7 The friction coefficient of sliding monolayers, as a function of the slip velocity. Slip velocities were calculated from Eq. 7 (■) and from the average displacements in Fig. 6 (●). The arrow denotes the effective friction coefficient ξ' of a slab of t_5 molecules with the same thickness as the bilayer (see text for details).

shows the distribution of longitudinal angles ϕ of the end-to-end vectors $\mathbf{r}_{15}$ of the amphiphiles, i.e., the orientation of the molecule in the plane of the bilayer. In the quiescent box this distribution is homogeneous, as expected for a bilayer in the liquid-crystalline or fluid L_α phase. The sheared system, on the other hand, reveals maxima at $\phi = 0$ and π rad, indicative of a propensity to tilt along the shear direction. A distribution of the tilt angles, defined as the angle θ between the z axis and the projection of $\mathbf{r}_{15}$ on the xz plane, is presented in Fig. 9. The two peaks of the distribution, corresponding to the upper and lower monolayer, lie at 0 and π rad in the quiescent box, and shift by $\Delta\theta$ under shear. This average tilt is proportional to the slip velocity and the overall shear rate. The length distribution of the end-to-end vectors is not affected by the shear flow.

It is interesting to note that for overall parallel shear rates beyond 0.05 τ^{-1}, which corresponds to a slip velocity of $\sim 11 \times 10^{-3} \sigma/\tau$, the bilayer becomes unstable. We observed

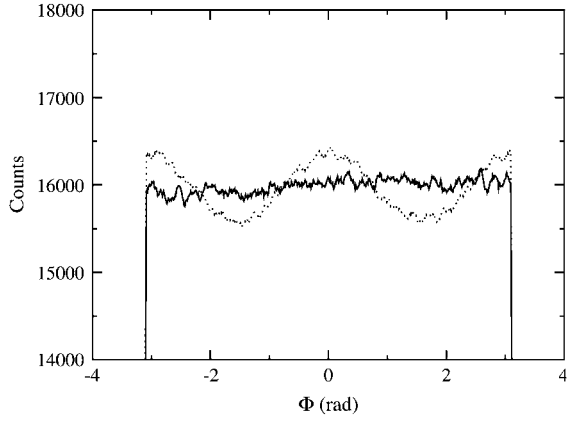

FIGURE 8 Histogram of the orientation of amphiphilic molecules in the plane of the bilayer. The solid line refers to a quiescent system, the dotted line to a parallel shear rate of $0.05\tau^{-1}$.

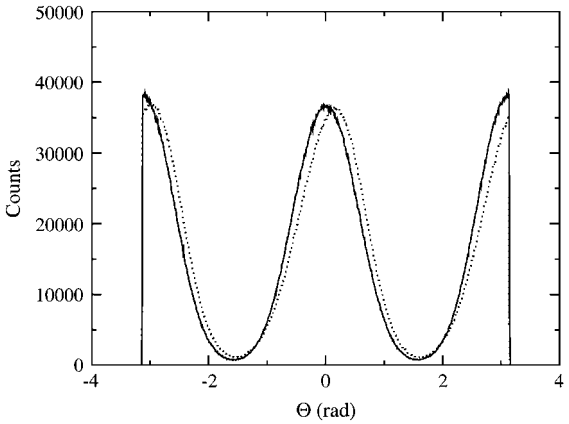

FIGURE 9 Probability distribution of the tilt of the amphiphiles in the flow direction. The solid line refers to a quiescent system, the dotted line to a parallel shear rate of $0.05\tau^{-1}$.

pronounced undulations of the bilayer, amphiphiles piling up to form buds, and the creation of transmembrane pores. Eventually the bilayer is torn apart. A further discussion of these phenomena will be presented elsewhere.

DISCUSSION AND CONCLUSIONS

The results of the preceding section show that nonequilibrium coarse-grained simulations can be used to study the flow characteristics of an amphiphilic bilayer, to wit, the bilayer viscosity η_s for coplanar shear deformations and the friction coefficient ξ between sliding monolayers. Both are obtained by placing the simulation box under a shear flow, with vorticity oriented perpendicular and parallel to the bilayer, respectively. The shear force acting on the bilayer is then easily obtained by subtracting the shear force on the solvent from the total shear force.

The common experimental method to obtain a surface viscosity is to measure the diffusion coefficient D of a tracer particle, a cylinder of radius a with a length equal to the bilayer thickness h_s. Assuming the bulk viscosity η_w of the surrounding solvent is much smaller (but not zero) than that of the bilayer, Saffman (17) derived that

$$D = \frac{k_B T}{4\pi\eta_s}\left[\ln\left(\frac{\eta_s}{a\eta_w}\right) - \gamma\right], \tag{8}$$

where k_B is Boltzmann's constant and $\gamma \approx 0.577$ is Euler's constant. In case $\eta_s/h_s \ll \eta_w$, this equation also holds when the tracer particle sticks out of the bilayer. Assuming that Eq. 8 may be used even at the molecular level, we set a equal to σ and find $D = 1.3 \times 10^{-2}\sigma^2/\tau$. Both from a direct calculation of the mean square displacements of the amphiphiles in a quiescent bilayer, as well as from the spreading of the distributions in Fig. 6, we find $D = 1.8 \times 10^{-2}\sigma^2/\tau$. Using half the surface viscosity in Eq. 8, because the diffusing amphiphiles span only half the bilayer (14), we get the same result. This agreement must be considered to be a bit fortuitous, of course. First, we have assumed that the radius of the flexible amphiphile is equal to σ, and thus includes the first ''solvation shell''. Second, the diffusion coefficient calculated from the Saffman equation is relatively insensitive to the surface viscosity, as illustrated by the two calculated values of D.

It is tempting to relate the viscosity η_s of the bilayer to the viscosity η_b of a bulk liquid of like molecules, in this case chains of five tail particles, t_5. This connection appears frequently in the literature (10,19), and is given by $\eta_s' = \eta_b h_s$. Inserting numerical values yields $\eta_s' = 14\epsilon^{1/2}m^{1/2}\sigma^{-1}$, which amounts to just over two-thirds of the actual value of η_s. This difference is due to the lower degree of ordering in the liquid relative to the bilayer, where the amphiphiles are stretched, aligned, and positioned in a near-planar configuration, and to the higher packing density in the bilayer made possible by this ordering.

The effective friction coefficient of a slab of t_5 with the same thickness as the bilayer is readily shown to be given by $\xi' = \eta_b/h_s$ (10,19). The resulting value of $\xi' = 0.3\epsilon^{1/2}m^{1/2}\sigma^{-3}$, indicated in Fig. 7 by an arrow, amounts to less than one-tenth of the actual bilayer friction coefficient. Here again, the increased ordering in the bilayer relative to the liquid must have caused the difference, which is much more pronounced for ξ than for η_s. Interestingly, on the basis of experimental data for the friction coefficient, Evans and Yeung and co-workers (10,11) also arrived at a mismatch by one order of magnitude.

We end with a brief comparison of our numerical results with experimental data. Whereas the model amphiphile possesses only one relatively short tail, experiments have concentrated on phosphatidylcholine PC lipids with two longer tails of typically 18 carbons. It is to be expected, therefore, that the latter yield considerably higher surface viscosities and friction coefficients than the model amphiphiles, even if friction and random forces had properly been included in the model. Reported surface viscosities for lipid bilayers (10,14,18) are of the order of 10^{-7}–10^{-6} surface poise (1 sp is equivalent to 10^{-3} Pa m s), as compared to the 8.5×10^{-10} sp found by the perpendicular shear simulations. Experimental friction coefficients are rare, with 1×10^8 N s m^{-3} reported by Evans and Yeung (10) and 4.5×10^8 N s m^{-3} by Raphael and Waugh (12). Chizmadzhev et al. (19) assumed in their analysis that $\eta_b = \xi' h_s = \eta_w'/h_s$; from their value of η_b we arrive at 2×10^9 N s m^{-3} for $h_s = 4$ nm. The parallel shear simulations yield 1.4×10^6 N s m^{-3} . In both cases, the simulation results are two to three orders of magnitude lower than the experimental values. As already alluded to, this is a consequence of using a simplified coarse-grained model, which does not discredit the proposed simulation method in any way.

This work is part of the SoftLink research program of the Stichting voor Fundamenteel Onderzoek der Materie (FOM), which is financially

supported by the Nederlandse Organisatie voor Wetenschappelijk Onderzoek (NWO).

REFERENCES

1. Gelbart, W. M., A. Ben-Shaul, and D. Roux. 1994. Micelles, Membranes, Microemulsions, and Monolayers. Springer-Verlag, New York, NY.
2. Seifert, U. 1997. Configurations of fluid membranes and vesicles. *Adv. Phys.* 46:13–137.
3. Evans, E., and V. Heinrich. 2003. Dynamic strength of fluid membranes. *C. R. Phys.* 4:265–274.
4. Rawicz, W., K. C. Olbrich, T. McIntosh, D. Needham, and E. Evans. 2000. Effect of chain length and unsaturation on elasticity of lipid bilayers. *Biophys. J.* 79:328–339.
5. Diat, O., D. Roux, and F. Nallet. 1995. ''Layering'' effect in a sheared lyotropic lamellar phase. *Phys. Rev. E.* 51:3296–3299.
6. Marlow, S. W., and P. D. Olmsted. 2002. The effect of shear flow on the Helfrich interaction in lyotropic lamellar systems. *Eur. Phys. J. E.* 8:485–497.
7. Panizza, P., A. Colin, C. Coulon, and D. Roux. 1998. A dynamic study of onion phases under shear flow: size changes. *Eur. Phys. J. B.* 4:65–74.
8. Sierro, P., and D. Roux. 1997. Structure of a lamellar phase under shear. *Phys. Rev. Lett.* 78:1496–1499.
9. Evans, E. A., and R. Skalak. 1980. Mechanics and Thermodynamics of Biomembranes. CRC Press, Boca Raton, FL.
10. Evans, E., and A. Yeung. 1994. Hidden dynamics in rapid changes of bilayer shape. *Chem. Phys. Lipids.* 73:39–56.
11. Evans, E., A. Yeung, R. Waugh, and J. Song. 1992. Dynamic coupling and nonlocal curvature elasticity in bilayer membranes. *Springer Proceedings in Physics.* 66:148–153.
12. Raphael, R. M., and R. E. Waugh. 1996. Accelerated interleaflet transport of phosphatidylcholine molecules in membranes under deformation. *Biophys. J.* 71:1374–1388.
13. Waugh, R. E. 1982. Surface viscosity measurements from large bilayer vesicle tether formation. Analysis. *Biophys. J.* 38:19–27.
14. Waugh, R. E. 1982. Surface viscosity measurements from large bilayer vesicle tether formation. Experiments. *Biophys. J.* 38:29–37.
15. Yeung, A., and E. Evans. 1995. Unexpected dynamics in shape fluctuations of bilayer vesicles. *J. Phys. II France.* 5:1501–1523.
16. Bates, F. S., and G. H. Fredrickson. 1990. Block copolymer thermodynamics: theory and experiment. *Annu. Rev. Phys. Chem.* 41:525–557.
17. Saffman, P. G. 1976. Brownian motion in thin sheets of viscous fluid. *J. Fluid Mech.* 73:593–602.
18. Dimova, R., C. Dietrich, A. Hadjiisky, K. Danov, and B. Pouligny. 1999. Falling ball viscosimetry of giant vesicle membranes: finite-size effects. *Eur. Phys. J. B.* 12:589–598.
19. Chizmadzhev, Y. A., D. A. Kumenko, P. I. Kuzmin, L. V. Chernomordik, J. Zimmerberg, and F. Cohen. 1999. Lipid flow through fusion pores connecting membranes of different tensions. *Biophys. J.* 76:2951–2965.
20. Essmann, U., and M. L. Berkowitz. 1999. Dynamical properties of phospholipid bilayers from computer simulation. *Biophys. J.* 76:2081–2089.
21. Groot, R. D., and K. L. Rabone. 2001. Mesoscopic simulation of cell membrane damage, morphology change and rupture by nonionic surfactants. *Biophys. J.* 81:725–736.
22. Kranenburg, M., J. P. Nicolas, and B. Smit. 2004. Comparison of mesoscopic phospholipid-water models. *Phys. Chem. Chem. Phys.* 108: 4142–4151.
23. Lindahl, E., and O. Edholm. 2000. Mesoscopic undulations and thickness fluctuations in lipid bilayers from molecular dynamics simulations. *Biophys. J.* 79:426–433.
24. Marrink, S. J., A. H. de Vries, and A. E. Mark. 2004. Coarse grained model for semiquantitative lipid simulations. *J. Phys. Chem.* 108:750–760.
25. Tieleman, D. P., S. J. Marrink, and H. J. C. Berendsen. 1997. A computer perspective of membranes: molecular dynamics studies of lipid bilayer systems. *Biochim. Biophys. Acta.* 1331:235–270.
26. den Otter, W. K., S. A. Shkulipa, and W. J. Briels. 2003. Buckling and persistence length of an amphiphilic worm from molecular dynamics simulations. *J. Chem. Phys.* 119:2363–2368.
27. Goetz, R., G. Gompper, and R. Lipowsky. 1999. Mobility and elasticity of self-assembled membranes. *Phys. Rev. Lett.* 82:221–224.
28. Goetz, R., and R. Lipowsky. 1998. Computer simulations of bilayer membranes: self-assembly and interfacial tension. *J. Chem. Phys.* 108: 7397–7409.
29. Tolpekina, T. V., W. K. den Otter, and W. J. Briels. 2004. Nucleation free energy of pore formation in an amphiphilic bilayer studied by molecular dynamics simulations. *J. Chem. Phys.* 121:12060–12066.
30. Tolpekina, T. V., W. K. den Otter, and W. J. Briels. 2004. Simulations of stable pores in membranes: system size dependence and line tension. *J. Chem. Phys.* 121:8014–8020.
31. Akkermans, R. L. C., and W. J. Briels. 2000. Coarse-grained dynamics of one chain in a polymer melt. *J. Chem. Phys.* 41:6409–6422.
32. Gardiner, C. W. 1985. Handbook of Stochastic Methods: For Physics, Chemistry and the Natural Sciences. Springer-Verlag, New York, NY.
33. Padding, J. T., and W. J. Briels. 2002. Time and length scales of polymer melts studied by coarse-grained molecular dynamics simulations. *J. Chem. Phys.* 117:925–943.
34. Smith, W., and T. R. Forester. 1996. dlpoly2.0: a general-purpose parallel molecular dynamics simulation package. *J. Mol. Graph.* 14: 136–141.
35. Allen, M. P., and D. J. Tildesley. 1987. Computer Simulation of Liquids. Oxford University Press, Oxford, UK.
36. Lees, A. W., and S. F. Edwards. 1972. The computer study of transport processes under extreme conditions. *J. Phys. C.* 5:1921–1929.
37. Holian, B. L. 2002. Evaluating shear viscosity: power dissipated versus entropy produced. *J. Chem. Phys.* 117:9567–9568.
38. Queimada, A. J., S. E. Quinones-Cisneros, I. M. Marrucho, J. A. P. Coutinho, and E. H. Stenby. 2003. Viscosity and liquid density of asymmetric hydrocarbon mixtures. *Int. J. Thermophys.* 24:1221–1239.